Journal of Zhejiang University-SCIENCE A (Applied Physics & Engineering)
ISSN 1673-565X (Print); ISSN 1862-1775 (Online)
www.jzus.zju.edu.cn; www.springerlink.com
E-mail: jzus@zju.edu.cn

Effect of relative humidity on non-refractory submicron aerosol evolution during summertime in Hangzhou, China*#

Ling-hong CHEN†1, Biao LV[1], Xian-jue ZHENG[2], Kang-wei LI[1], Jian-dong SHEN[2], Kai-ji BAO[1], Xue-cheng WU[1], Cheng-hang ZHENG[1], Fang YING[2], Xiang GAO[1], Ke-fa CEN[1]

[1]*State Key Laboratory of Clean Energy Utilization, Zhejiang University, Hangzhou 310027, China*

[2]*Hangzhou Environmental Monitoring Center Station, Hangzhou 310007, China*

†E-mail: chenlh@zju.edu.cn

Received May 24, 2017; Revision accepted Dec. 10, 2017; Crosschecked Dec. 15, 2017

Abstract: Relative humidity (RH) has a significant and complex effect on aerosols because of the aqueous phase process and gas-particle partition. The mass concentration and size distribution of organic aerosols, sulfate, nitrate, ammonium, and chloride were measured using high-resolution time-of-flight aerosol mass spectrometry (HR-ToF-AMS). These measurements were recorded from Aug. 5 to Sept. 23, 2016 in Binjiang District, Hangzhou, China, during which period more than 78% of the readings showed an RH over 60%, while the average temperature was 26 °C. Correlation analysis was applied to inorganic aerosol measurements while positive matrix factorization (PMF) was applied for source apportionment of organic aerosols (OA). The pattern of fixation of ammonium in aerosols changed as the RH increased, suggesting that RH enhances nitrate participation in particles, while sulfate is scavenged by droplets. All species of non-refractory submicron particles (NR-PM_1) showed an increase in their peak size as the RH increased. Primary OA (POA) continuously accumulated as the RH increased. When RH<60%, oxygenated OA (OOA) increased with increasing RH because of oxidation; semi-volatile OOA (SV-OOA) had a higher mass concentration during the daytime than at nighttime, indicating that the aqueous phase process and photochemistry synergistically affect the formation of oxygenated SV-OOA. When RH>60%, there was a relatively slow decrease in OOA, dominated by the wet removal effect rather than oxidation. The degree of oxidation of OA decreased as RH increased; this can be explained by most of the OOA with higher hygroscopicity being removed as droplets.

Key words: Relative humidity (RH); Aerosol composition; Size distribution; Wet removal; Aqueous-phase
https://doi.org/10.1631/jzus.A1700567 **CLC number:** TV5

1 Introduction

Atmospheric aerosols markedly affect the radiative balance in the Earth's atmosphere and play a central role in climate (Solomon, 2007; Tong et al., 2015, 2016a, 2016b, 2017). They also have a significant impact on human health (Davidson et al., 2005). Submicron particles (PM_1, aerodynamic diameter less than 1 μm) have a greater effect on the environment and human health because of their longer lifetime and smaller gravity settlement effect and a greater effect since they penetrate deeper into the lungs. Aerosols contain organic and inorganic compounds, and organic aerosols (OA) play a major role in fine particles (Kanakidou et al., 2005; Zhang et al., 2007a). Organic aerosols can be divided into primary organic aerosol (POA) and secondary organic aerosol (SOA). POA is direct outputs from pollutant sources such as vehicles and plants, while SOA is formed by nucleation,

* Project supported by the Project of Hangzhou G20 Environmental Protection (No. 2016-004), the Project of Hangzhou Technology (No. 20160533B85), the Public Project of Ministry of Environmental Protection (No. 201409008-4), the National Basic Research Program of China (No. 2015CB251501), the Program of Introducing Talents of Discipline to University (No. B08026), and the Innovative Research Groups of the National Natural Science Foundation of China (No. 51621005)

Electronic supplementary materials: The online version of this article (https://doi.org/10.1631/jzus.A1700567) contains supplementary materials, which are available to authorized users

ORCID: Ling-hong CHEN, https://orcid.org/0000-0002-8171-4632

condensation, and heterogeneous reaction of precursors (Canagaratna et al., 2007). However, the uncertainties around aerosol properties and the mechanism of aerosol formation make their effects unpredictable.

It is well known that relative humidity (RH) plays an important role in the chemical composition, size distribution, and optical properties of aerosols (Day and Malm, 2001; Hallquist et al., 2009; Sun et al., 2013; Gilardoni et al., 2014). RH affects aerosol formation in different ways, such as via gas-particle partition and the aqueous phase reaction. Seinfeld et al. (2001) suggested that water condensed on particles due to increasing RH favors SOA condensation, especially with the participation of semi-volatile water-soluble organic components (WSOC), i.e. the gas-particle partition coefficient is influenced by RH, and SOA production is elevated, followed by further oxidation (Hennigan et al., 2009). Lim et al. (2010) and Ervens et al. (2011) suggested that oxidation processes in the aqueous phase might contribute almost as much mass as the gas phase. Fog events are defined by liquid water content in the absence of visibility measurements in several studies (Gilardoni et al., 2014; Chakraborty et al., 2016). By comparing SOA formation on foggy days and non-foggy days, Kaul et al. (2011) suggested that the enhanced SOA production on foggy days is due to the aqueous phase process, while aerosol acidity is increased by the oxidation of SO_2. Ge et al. (2012) supported the conclusion that fog processes enhance SOA production and the degree of oxidation. Collett et al. (2008) showed that fog scavenging reduces aerosol loading by promoting wet removal. It is worth mentioning that most fog processes are studied during the winter, in the temperature range from −5 °C to 20 °C (Sun et al., 2006; Kaul et al., 2011; Ge et al., 2012).

Non-refractory PM_1 (NR-PM_1) can be measured by high-resolution time-of-flight aerosol mass spectrometry (HR-ToF-AMS), which provides the mass concentration and size distribution of organic mass, sulfate, nitrate, ammonium, and chloride (Jayne et al., 2000; Decarlo et al., 2006; Canagaratna et al., 2007; Jimenez et al., 2009). Recent advances in analytical methods for aerosol mass spectrometry (AMS) data and PMF factors provide a platform for further research on aerosols (Lanz et al., 2007; Ulbrich et al., 2008; Zhang et al., 2011).

The time scale of the oxidation process for different sources is reported in few studies. The potential aerosol mass (PAM) oxidation flow reactor (OFR) was developed and used for the measurement of the time scale of the oxidation process (Tkacik et al., 2014; Ortega et al., 2016). Aging measurements of vehicular exhaust in a highway tunnel indicated peak SOA production after 2.5 d of atmospheric equivalent photochemical aging (Tkacik et al., 2014). A fit of field and reactor data result in a timescale of SOA formation of about 0.3 d and fragmentation-dominated heterogeneous oxidation and net mass loss with a timescale of about 50 d in the Los Angeles area. These evidences support for hourly RH measurement to explore the oxidation process.

In the present study, HR-ToF-AMS was used to measure and analysis PM_1 in Hangzhou in summer, with a mean temperature of 26 °C, higher than those in other studies. The effect of RH on the evolution and size distribution of submicron aerosols, including organic and inorganic species, is explored here.

2 Methods

2.1 Sampling

Field measurements were conducted in an environmental monitoring station (on the roof of an eight-floor building) in Binjiang District (30°12′29.6″ N, 120°12′43.3″ E), Hangzhou. NR-PM_1 were measured in situ by a HR-ToF-AMS. The observations were continuously recorded from Aug. 5, 2016 to Sept. 23, 2016 excepting calibration and maintenance periods. A $PM_{2.5}$ cyclone (URG-2000-30ED, Aerodyne Research Inc., USA) and half inch copper tube were used to induce the sample into the AMS. The sample was dried via a Nafion tube (Dryer-50, Aerodyne Research Inc., USA) before the inlet.

The HR-ToF-AMS was operated in mass-sensitive V-mode and high-mass-resolution W-mode in alternating 5-min periods. In V-mode, the AMS cycled through the mass spectrum (MS) and efficient particle time-of-flight (ePToF) modes every 10 s. In W-mode, no ePToF data were collected due to the limited signal-to-noise (S/N) ratio. Meteorological parameters such as solar radiation, RH, temperature, and gas species including CO, NO_2, SO_2, and O_3 were

measured contemporaneously. These data were provided by the environmental monitoring station. These data as a function of RH are shown in Fig. S1.

2.2 Data analysis

The HR-ToF-AMS measured the mass concentration and chemical composition of NR-PM_1 species. The unit mass spectrum data were analyzed using a ToF-AMS Analysis Toolkit (SQUIRREL, 1.57I); the high-resolution data were analyzed with ToF-AMS HR Analysis (PIKA, 1.16I). In particular, the collection efficiency (CE) was improved by the method of Middlebrook (Middlebrook et al., 2012), which was used to account for AMS detection efficiency that is mainly caused by the particle bounce effects at the vaporizer (Matthew et al., 2008). Positive matrix factorization (PMF) was performed on AMS organic aerosol HR mass spectra (*m*/*z* 12–120) to retrieve potential components with different sources and processes (Paatero and Tapper, 1994). The results of PMF were further evaluated using an Igor Pro (6.37.2)-based PMF Evaluation Tool (PET, v2.08D) (Ulbrich et al., 2008). Four OA components were identified: low-volatility oxygenated OA (LV-OOA), semi-volatility oxygenated OA (SV-OOA), hydrocarbon-like OA (HOA), and cooking OA (COA). More details about these four components are shown in Fig. S2, including their mass spectral profiles and time series. These suggest their different source characteristics and processes.

The liquid water content (LWC) was calculated by the ISORROPIAII model (http://isorropia.eas.gatech.edu/index.php?title=Code_Repository). The LWC as a function of RH is also shown in Fig. S1. The input aerosol inorganic data (sulfate, nitrate, ammonium, and chlorine) are derived from the AMS data.

3 Results and discussion

3.1 RH impact on aerosol components

The mass concentration and mass fraction of the NR-PM_1 and OA components are shown as functions of the RH in Fig. 1. In Fig. 1, the mass concentration of sulfate when RH<60% showed a significant difference between daytime and nighttime. When

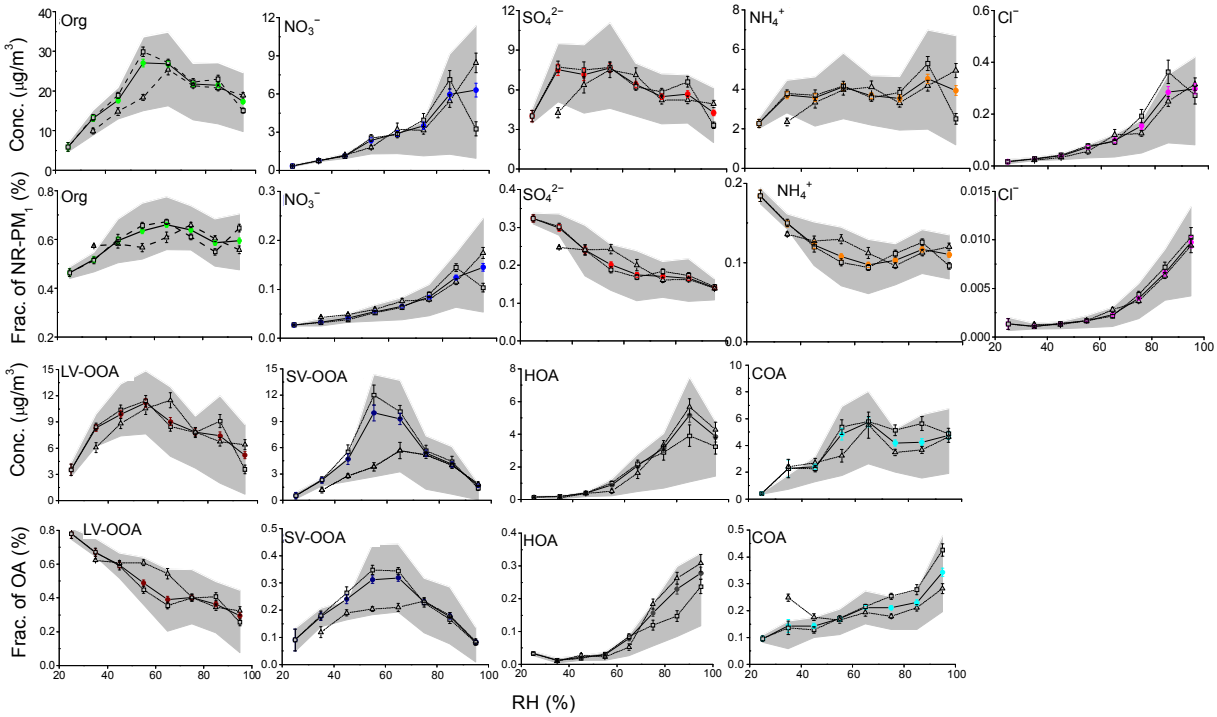

Fig. 1 Variation of mass concentration and mass fraction of NR-PM_1 and OA species as a function of RH

Data are grouped in RH bins with 10% increments. The shaded areas indicate the 25th and 75th percentiles. The solid colored circles, white squares, and white triangles refer to the mean, day mean, and night mean, respectively. Org: organic

RH>60%, the mean values are similar, suggesting that photooxidation may influence sulfate formation at lower RH values. However, Fig. 1 shows that nitrate has almost the same mean value during day and night, suggesting that photooxidation of nitrate is probably not as important as other oxidation mechanisms. Nitrate shows a similar variation with NO_2 in Fig. S1, indicating that NO_2 emission enhances the nitrate formation. More details are discussed in Section 3.3. The relative proportions of NR-PM_1 components are shown in Fig. 2. Organic compounds form a dominant proportion, and are elevated as RH increases when RH<60%, but their relative proportion begins to fall as RH increases above 60%. The nitrate fraction increases from 2.7% to 14.5%; at the same time, the nitrate mass concentration also increases. This indicates that the aqueous phase process might play a significant role in nitrate formation. The sulfate fraction of NR-PM_1 continuously decreases from 32.4% to 14.0% as the RH increases, and the sulfate mass concentration also decreases in general. The trend shown for sulfate in NR-PM_1 is opposite to that found by Sun (2013); however, the conditions are totally different. The mass concentration of chlorine is about 0.3 μg/m^3, and its fraction is about 1%. Chlorine was too small to see variations. Ammonium shows a weaker dependency on RH; the fixation of ammonium is associated with sulfate and nitrate and is discussed in more detail in Section 3.3. It can be seen from Fig. S1 that LWC shows a growth trend as RH increases, possibly indicating that wet removal is responsible for organic aerosol reduction even for NR-PM_1 (Collett et al., 2008). Fig. 1 shows that the mass concentrations and mass fractions of chlorine and nitrate have a similar growth trend as RH increases. The data obtained when RH<30% are a little deficient in this study; however, RH<30% is shown for comparison to other conditions of RH.

The proportions of the OA factors are shown in Fig. 3. The fraction of LV-OOA continuously decreases as RH increases, so wet removal mainly acts on more oxygenated and aged aerosols caused by their higher hygroscopicity. LV-OOA shows the same tendency as sulfate, consistent with sulfate being influenced by wet removal. The mass concentration and fraction of SV-OOA are similar to those of organics in NR-PM_1.

When RH<60%, all OA components' mass concentration (SOA and POA) increase with RH, and the POA (HOA and COA) shows a weaker relationship with RH. Although the mass concentrations of SV-OOA and LV-OOA both increase with RH, O_3 shows a continuous decreasing with RH elevated in Fig. 2, supporting the view that O_3 oxidation could not play a significant role. LV-OOA and SV-OOA mass fractions show the opposite tendency, suggesting that the increase in organic mass is dominated by SV-OOA. It should be noted that the daytime mean of SV-OOA is obviously higher than the nighttime mean, indicating that photochemical oxidation is important for the formation of SV-OOA.

When RH>60%, the daytime mean and nighttime mean of SV-OOA become closer, so the decrease in SV-OOA is not obviously affected by light. It is possible that the wet removal effect overwhelms the SV-OOA formation. The OOA (SV-OOA and LV-OOA) mass concentration begins to fall as RH increases; this phenomenon can be explained because OOA has greater hygroscopicity leading to more efficient scavenging. The nighttime mean of HOA is higher than the daytime mean, which means that the HOA mass growth rate in the daytime is slower than that at nighttime, because HOA is more oxygenated and aged by photochemical reactions. Meanwhile, the increasing degree of oxidation of OA will increase their hygroscopicity, followed by their participation with water particles (Wong et al., 2011).

3.2 RH impact on aerosol distribution

The size distribution of NR-PM_1 species divided at RH=60% is shown as a unimodal distribution in Fig. 4, where D_{va} means the aerodynamic diameter, and M means the mass concentration. The mass concentration of chlorine is close to zero, so it cannot show a variation. However, the peak particle diameter of other species (about 600 nm) when RH>60% is larger than the peak size (about 500 nm) when RH<60%, indicating that increased RH enhances particle size growth. Both peak sizes belong to the accumulation mode (50 nm<D_{va}<2000 nm) (Decarlo et al., 2004).

As shown in Table 1, organics have a lower peak size mass concentration at RH>60%, as does sulfate, possibly suggesting that they are internally mixed with each other and simultaneously scavenged by wet removal (Gilardoni et al., 2014). This explanation is

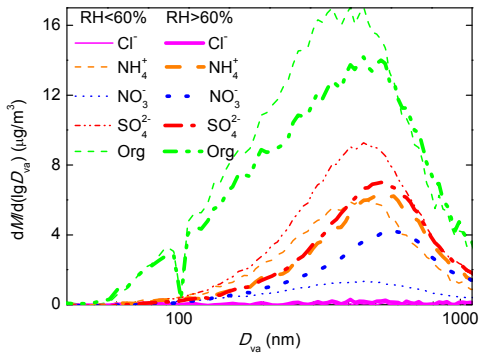

Fig. 4 Size distributions of NR-PM$_1$ components divided at RH=60%

consistent with the data shown in Fig. 3. The peak size mass concentrations of nitrate, ammonium, and chlorine show different extents of growth. Variation in nitrate is the greatest, which seems to suggest that

Table 1 Peak size mass concentration

Species	Peak size mass concentration (μg/m^3)	
	RH<60%	RH>60%
Organic	17.03	14.19
Sulfate	9.29	7.00
Nitrate	1.33	4.29
Ammonium	6.02	6.42
Chlorine	0.12	0.31

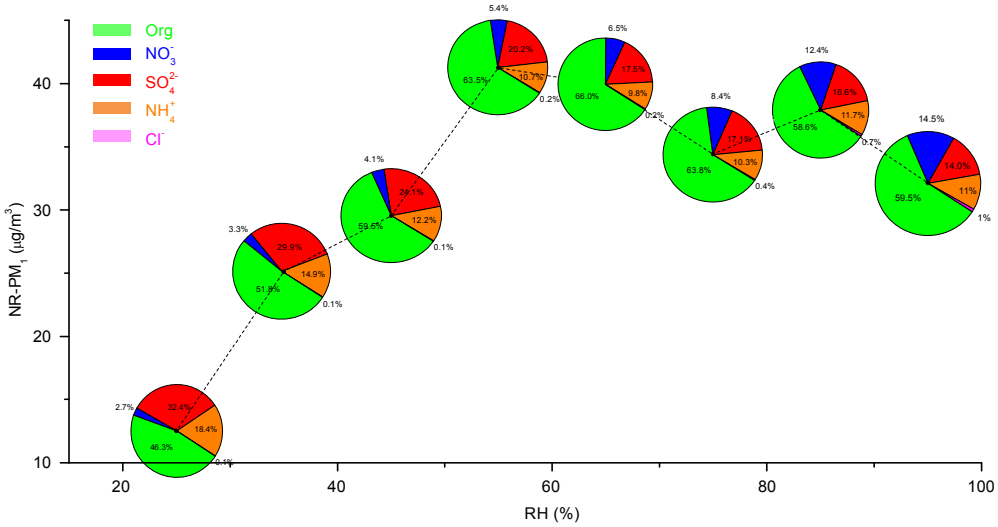

Fig. 2 Variation of mass concentrations of NR-PM$_1$ and composition of the species fraction as a function of RH. Data are grouped in RH bins with 10% increments

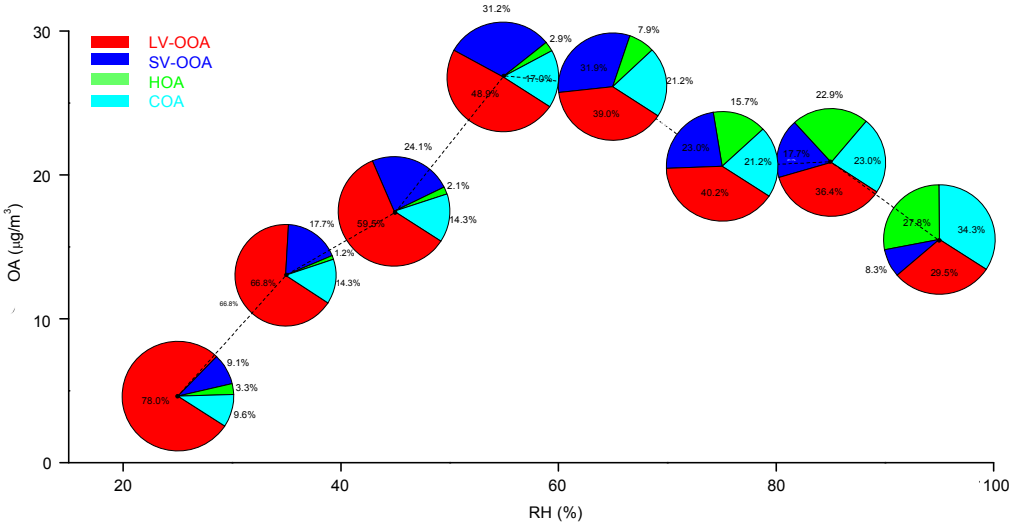

Fig. 3 Variation of OA mass concentrations and four PMF factors fraction as a function of RH. Data are grouped in RH bins with 10% increment

the effect of the aqueous phase process or water-taken participation of nitrate is vital in this study.

Fig. S3 explores the size distribution varying with RH, and presents a different picture compared with the size distribution over time, where the size increases smoothly and continuously. RH does not increase continuously with time, so these pictures are full of burrs. Fig. S3 shows that the variation of RH seems to have little effect on the size distribution of organics, sulfate, and ammonium. There is no apparent variation in chlorine due to its tiny mass concentration. For the size distribution of nitrate, high RH has an obvious effect on mass concentration while low RH does not, supporting the idea that the aqueous phase process or water-taken participation may promote the size growth of nitrate-containing NR-PM_1.

3.3 RH impact on inorganic

The formation of sulfate and nitrate will increase the acidity of aerosol particles. Acidity is an important factor for the secondary particle formation (Gao et al., 2004). NR-PM_1 particle acidity is evaluated by the ratio of the measured NH_4^+ to predicted NH_4^+, as NH_4^+ should be neutralized by SO_4^+, NO_3^-, and Cl^- with other metal cations and organic acids removing a little (Zhang et al., 2007). Eq. (1) is used to calculate the predicted NH_4^+:

$$m_{\mathrm{NH_4^+(pred.)}} = 18\times\left(\frac{m_{\mathrm{SO_4^{2-}}}}{96}\times 2+\frac{m_{\mathrm{NO_3^-}}}{62}+\frac{m_{\mathrm{Cl^-}}}{35.5}\right), \quad (1)$$

where $m_{\mathrm{NH_4^+(pred.)}}$, $m_{\mathrm{SO_4^{2-}}}$, $m_{\mathrm{NO_3^-}}$, and $m_{\mathrm{Cl^-}}$ are the mass concentrations of predicted NH_4^+, SO_4^{2-}, NO_3^-, and Cl^-, respectively. Fig. 5 shows the ratio of measured NH_4^+ to predicted NH_4^+ when RH>60%, when RH<60%, and over the total range. All ratios are about 1.1 with a Pearson coefficient about 0.99, without other metal ion information and considering the limit of non-refractory at 600 °C by tungsten. The results suggest that the NR-PM_1 particles are slightly alkaline and their pH is little affected by RH in this research. The regression line is for those upper points, and its slope has a large value of about 1.5. Since this is abnormal for field data, we consider those data as mistaken points.

The sulfur to oxidation ratio (SOR) is an important way to study sulfate formation, which is also expressed by the fraction of sulfate to total sulfur ($F_{\mathrm{SO_4^{2-}}}$), i.e.

$$F_{\mathrm{SO_4^{2-}}} = \frac{C_{\mathrm{SO_4^{2-}}}}{C_{\mathrm{SO_4^{2-}}}+C_{\mathrm{SO_2}}}, \quad (2)$$

where $C_{\mathrm{SO_4^{2-}}}$ and $C_{\mathrm{SO_2}}$ are the molar concentrations of SO_4^{2-} and SO_2, respectively. $F_{\mathrm{SO_4^{2-}}}$ is shown as a function of RH in Fig. 6a. The nitrogen to oxidation ratio (NOR) is similar to the SOR and the total nitrogen is considered as the sum of NO_2 and nitrate (Fig. 6b, Eq. (3)).

$$F_{\mathrm{NO_3^-}} = \frac{C_{\mathrm{NO_3^-}}}{C_{\mathrm{NO_3^-}}+C_{\mathrm{NO_2}}}, \quad (3)$$

where $C_{\mathrm{NO_3^-}}$ and $C_{\mathrm{NO_2}}$ are the molar concentrations of NO_3^- and NO_2, respectively. The higher the SOR and NOR are, the greater the oxidation of gases and the more secondary aerosols are present in the atmosphere. The SOR and NOR average values were 0.258±0.105 and 0.100±0.093, comparable with the results of Fu et al. (2008) that were recorded during days of good weather in Shanghai. This phenomenon can be explained by the fact that the total emission level is lower during this period. NOR has a range of 0.007–0.193. This variation cannot be neglected in evaluating the nitrate formation formed by NO_2.

SO_2 is converted to sulfate, which then participates in particle formation by two main routes: in low

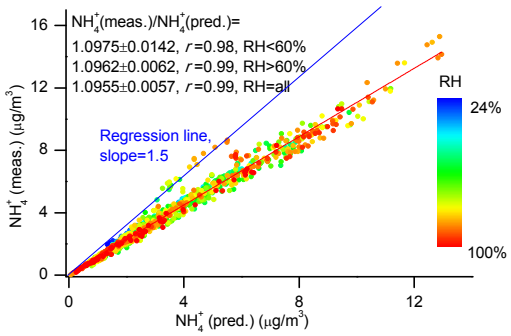

Fig. 5 Correlation between the measured and predicted NH_4^+ (*r* is the Pearson coefficient)

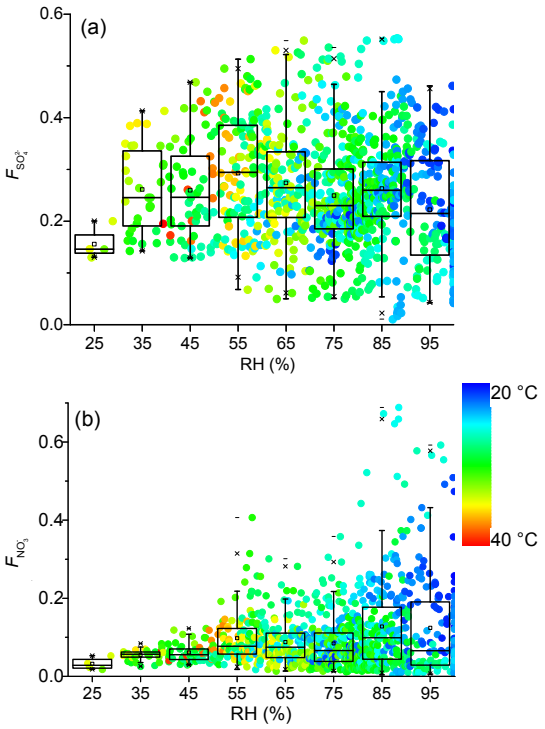

Fig. 6 $F_{SO_4^{2-}}$ and $F_{NO_3^-}$ as a function of RH, temperature is shown as the color bar. The upper and lower "–" markers are maximum and minimum values; the "×" markers above and below the whiskers represent the 99th and 1st percentiles; the whiskers above and below the boxes are the 90th and 10th percentiles; the upper and lower boundaries of the boxes indicate the 75th and 25th percentiles; the lines and the dots inside the boxes are the median and mean values, respectively

RH, sulfate is predominantly formed by reacting with OH radicals in the gas phase; in high RH, sulfate is formed mainly by reacting with oxidants (such as O_3 and H_2O_2) in the aqueous phase, when the aqueous process rate is almost an order of magnitude higher (Middleton et al., 1980; Saxena and Seigneur, 1987; Seigneur and Saxena, 1988; Seinfeld and Pandis, 2012; Shen et al., 2012). The formation of nitrate is more complex as there are many nitrogen-containing species that are interconverted in the atmosphere (NO, NO_2, N_2O_5, etc.). Hydrolysis of N_2O_5 is favored by water content and acidity. Sun et al. (2013) showed an outstanding increase of SOR and NOR with increasing RH in winter in Beijing. However, in the present study the SOR and NOR vs. RH relationships shown in Fig. 6 have obscure functions, which cannot be fitted as in (Sun, 2013). The formation of sulfate and nitrate cannot be simply explained by the aqueous-phase process and the enhancement of hydrolysis of N_2O_5. Factors contributing to SOR and NOR are complicated. For example, Pathak (2009) indicated that nitrate formation is related to aerosol pH, aerosol water, aerosol mass, and total reactive nitrogen in a study of Beijing and Shanghai. These parameters are believed to be important to heterogeneous chemistry, and therefore deserve further detailed research.

The relationship between $C_{NO_3^-}/C_{SO_4^{2-}}$ and $C_{NH_4^+}/C_{SO_4^{2-}}$ is used to study $C_{NO_3^-}$ and $C_{NH_4^+}$ at different $C_{SO_4^{2-}}$ levels, and is indicative of the pathway of the reaction between ammonia and nitric acid and other formation processes of nitrate in different concentrations of sulfate (Pathak et al., 2004, 2009; Huang et al., 2011; He et al., 2012; Squizzato et al., 2013). The regression equation of Fig. 7a is

$$\frac{C_{NO_3^-}}{C_{SO_4^{2-}}} = 0.85 \times \frac{C_{NH_4^+}}{C_{SO_4^{2-}}} - 1.94. \quad (4)$$

The intercept with the *x*-axis (i.e. $C_{NH_4^+}/C_{SO_4^{2-}}$) is 2.28. This intercept is different from 1.5 (Pathak et al., 2004; Huang et al., 2011), because it is relative to other inorganic salts and requires further study to verify its accuracy. Pathak et al. (2004, 2009) defined the excess $C_{NH_4^+}$ as

$$\text{Excess } C_{NH_4^+} = \left(\frac{C_{NH_4^+}}{C_{SO_4^{2-}}} - 2.28 \right) \times C_{SO_4^{2-}}. \quad (5)$$

Fig. 7b shows that the regression slope is 0.91 with the Pearson coefficient of 0.97. That this slope is close to 1 indicates that the excess $C_{NH_4^+}$ is almost completely neutralized by nitrate and chloride. Pathak et al. (2004, 2009) reported that when $C_{NH_4^+}/C_{SO_4^{2-}} > 1.5$, i.e. excess $C_{NH_4^+} > 0$ in rich-ammonium region, increases of nitrate via the gas-phase homogeneous reaction between ambient ammonia and nitric acid are significant. In a poor-ammonium region, heterogeneous reactions not involving NH_3 predominate, are most

likely the hydrolysis of N_2O_5 on preexisting aerosols (Pathaket al., 2009). The data in the present study are from an ammonium-rich region, suggesting that gas-phase homogeneous reaction overwhelms the hydrolysis of N_2O_5 in nitrate formation.

The correlations of sulfate and nitrate with ammonium partitioned and colored by the RH are shown in Figs. 8 and 9. The Pearson coefficient of sulfate with ammonium decreases slightly as RH increases, suggesting that ammonium in particles is preferably in the form of ammonium sulfate ($(NH_4)_2SO_4$) at low RH while the slightly alkaline conditions exclude the formation of NH_4HSO_4.

Conversely, the Pearson coefficient of nitrate

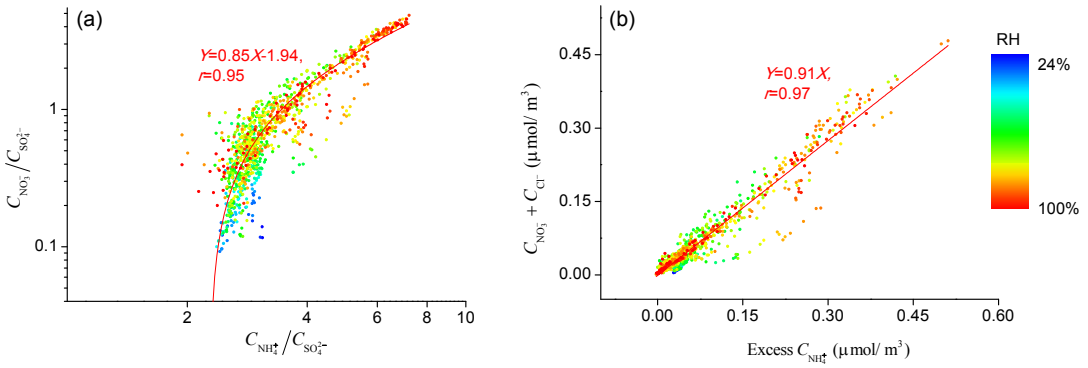

Fig. 7 Relationship of $C_{NH_4^+}$ with other inorganic species

(a) Correlation between the molar ratio $C_{NH_4^+}/C_{SO_4^{2-}}$ and $C_{NO_3^-}/C_{SO_4^{2-}}$; (b) Correlation between excess $C_{NH_4^+}$ and $C_{NO_3^-}+C_{Cl^-}$

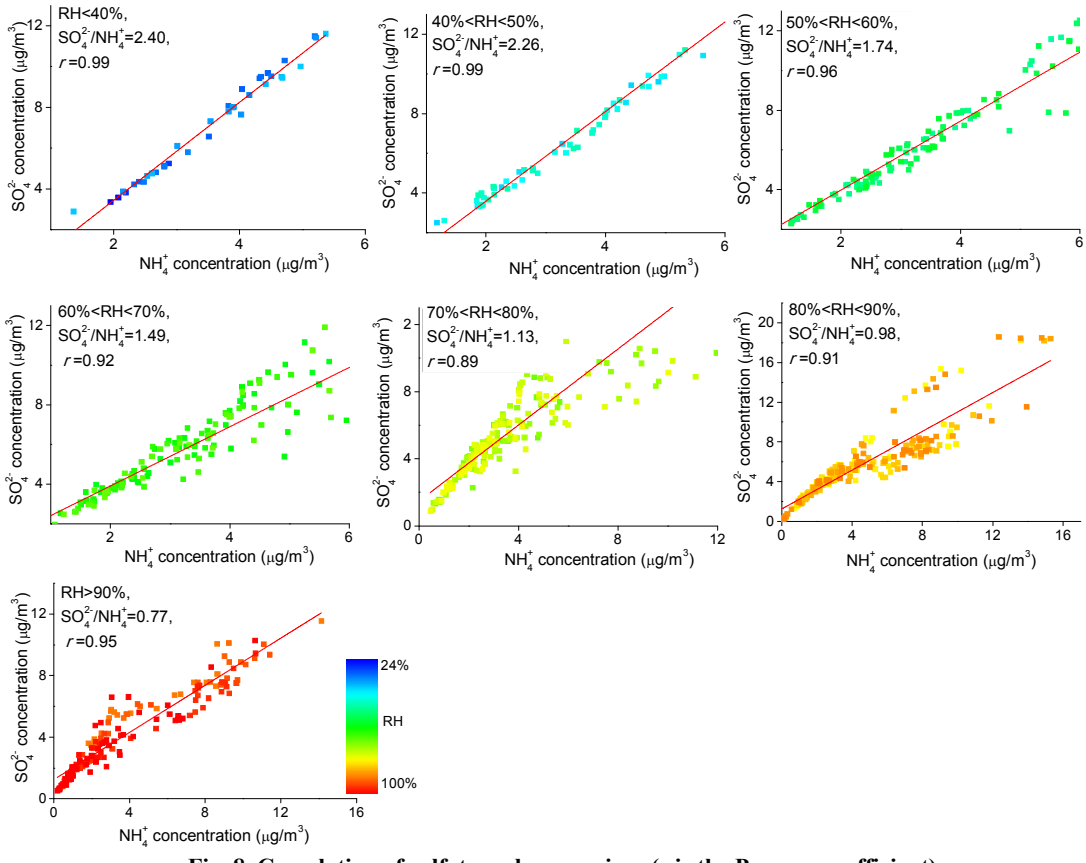

Fig. 8 Correlation of sulfate and ammonium (*r* is the Pearson coefficient)

increases as RH increases (except in the range 40%<RH<50%), indicating that ammonium nitrate (NH_4NO_3) as the dominant form participates in aerosols as the RH increases. In general, the Pearson coefficients of sulfate and ammonium remain at a high level (about 0.9) over the whole RH range while those of nitrate and ammonium show a very significant change as the RH increases. This is most likely a consequence of the fact that $(NH_4)_2SO_4$ is the dominant form for ammonium fixation in aerosols, while increasing the RH enhances aerosol NH_4NO_3 formation.

It is notable that the ratio of sulfate to ammonium decreases as the RH increases. According to the formulae of $(NH_4)_2SO_4$ and NH_4NO_3, the corresponding relative molecular mass ratios ($m_{SO_4^{2-}}/m_{NH_4^+}$ and $m_{NO_3^-}/m_{NH_4^+}$) are 2.67 and 3.44. As Table 2 shows, the maximum ratios are 2.40 and 2.07. It should be noticed that the maximum ratios

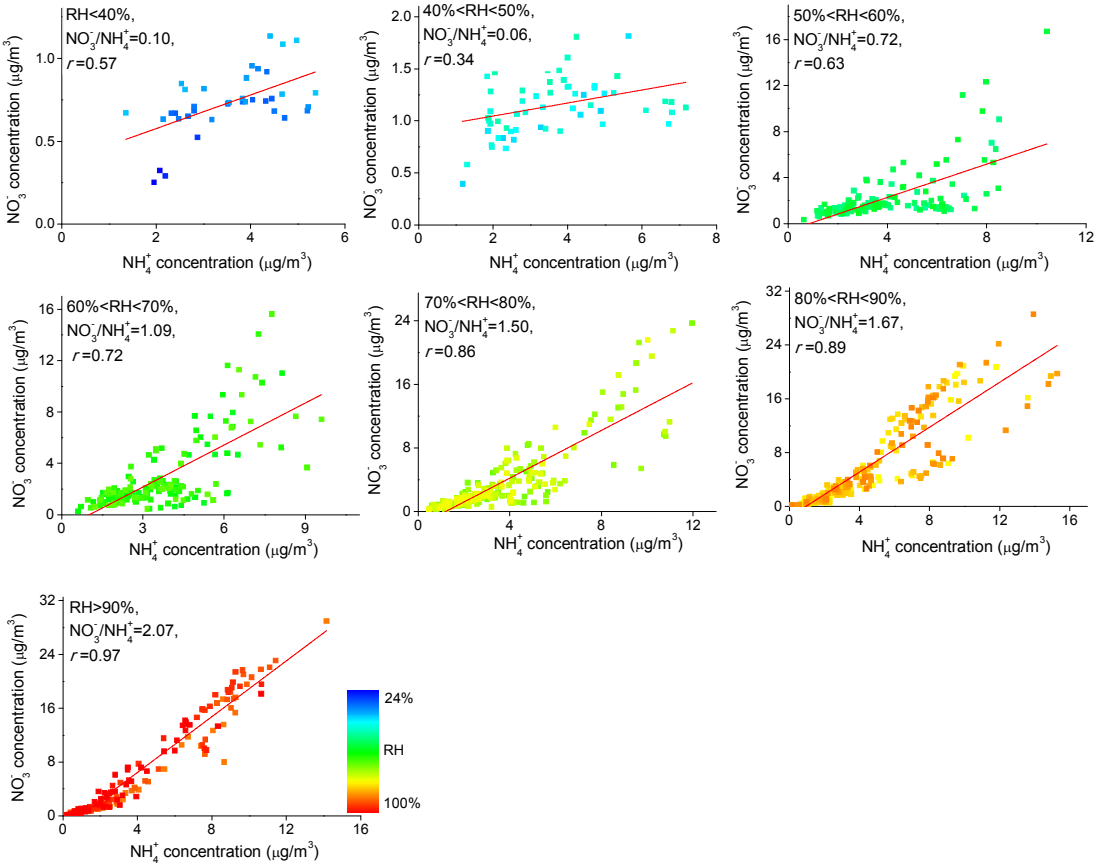

Fig. 9 Correlation of nitrate and ammonium (*r* is the Pearson coefficient)

Table 2 Regression line slope

RH	$m_{SO_4^{2-}}/m_{NH_4^+}$	$m_{NO_3^-}/m_{NH_4^+}$	$(m_{SO_4^{2-}}+m_{NO_3^-})/m_{NH_4^+}$
RH<40%	2.40	0.10	2.50
40%<RH<50%	2.26	0.06	2.32
50%<RH<60%	1.74	0.72	2.46
60%<RH<70%	1.49	1.09	2.58
70%<RH<80%	1.13	1.50	2.63
80%<RH<90%	0.98	1.67	2.65
RH>90%	0.77	2.07	2.84

are in different RH bins, but the ratios summation seems to increase with the increase of RH. Probably the nitrate makes up for or even exceeds the loss of ammonium fixed by sulfate. The mass concentration of ammonium is supposed not to be influenced by RH as shown in Fig. 1. Based on the hypothesis that ammonium is constant in this study, it can be concluded that sulfate is indeed decreasing and nitrate increasing as the RH increases. Possibly the aqueous-phase reaction enhances the nitrate mass and sulfate is scavenged by droplets in particles. Furthermore, NH_4NO_3 is produced by the gas-phase homogeneous reaction and RH enhances its participation in particles.

3.4 Impact of RH on organics

The signal fraction of OA from the AMS spectrum can reflect some variations in OA. In AMS the fragments such as *m*/*z* 43, *m*/*z* 44, and *m*/*z* 57 are the signal that can be detected, and it also has a total organic aerosol signal (OA). f43 (fraction of *m*/*z* 43) can be calculated by

$$\mathrm{f43} = (m/z\ 43)/\mathrm{OA}. \tag{6}$$

f44 and f57 can be calculated by similar method. f44 and f57 have been widely used as tracers for OOA (SV-OOA and LV-OOA) and HOA, with little effect of biomass burning. OOA is considered as a surrogate of the secondary OA; the others are supposed to be surrogates of primary OA (Ulbrich et al., 2008; Aiken et al., 2009; Ng et al., 2011b). f43 plays an important role in distinguishing SA-OOA from LV-OOA (Ng et al., 2010), as LV-OOA has a higher O/C ratio (i.e. oxidation degree) and lower volatiles than SV-OOA. The aging of OA leads to a decrease in f43 and volatiles, and increases in f44, the O/C ratio, and hygroscopicity (Jimenez et al., 2009; Ng et al., 2010). f60 is used as a tracer of biomass burning (Schneider et al., 2006; Alfarra et al., 2007), and other organic aerosols like carboxylic acids and cooking emissions also contribute to the f60 signal (Decarlo, 2008; Mohr et al., 2009; Aiken et al., 2010; He et al., 2010).

As shown in Fig. 10, f60 forms a constant proportion of the aerosols at around 0.1%–0.2%. The background values measured by Decarlo (2008) and Aiken et al. (2009) are about 0.3%. Meanwhile, our PMF results show no biomass burning organic aerosol (BBOA) factor, so biomass burning in this study had little effect on OA. f43 shows a similar trend with organics but with less variation. f44 falls as RH increases, and it can be concluded that the OOA especially LV-OOA undergoes wet scavenging with

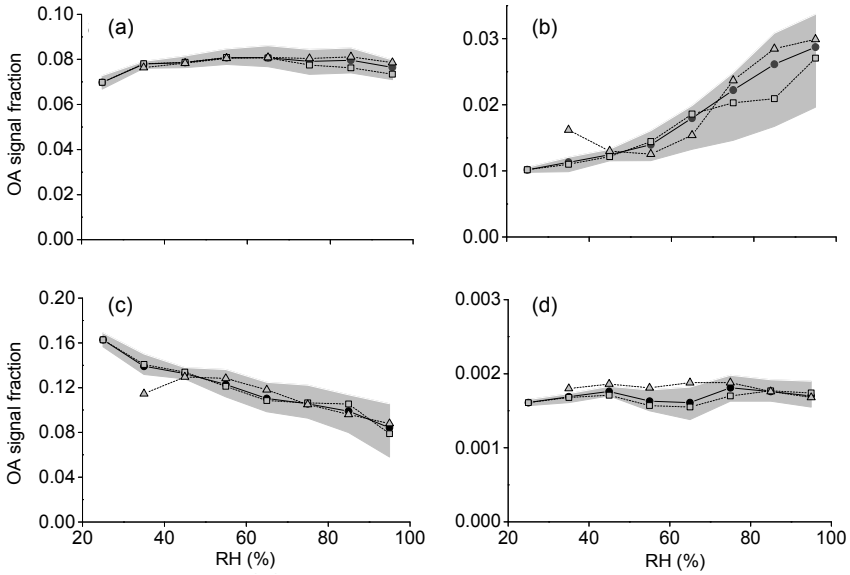

Fig. 10 Variation of the specific fraction of OA signal as a function of RH: (a) f43; (b) f57; (c) f44; (d) f60
Data are grouped in RH bins with 10% increments. The shaded areas indicate the 25th and 75th percentiles. The solid colored circles, white squares, and white triangles show the mean, daytime mean, and nighttime mean, respectively

increasing RH. However, f57 presents an opposite trend, with f57 increasing as f44 decreases, indicating that an RH increase may enhance the POA participation in particles, especially for some water-soluble components. In addition, increasing RH leads to more efficient wet removal of OOA, especially LV-OOA.

A plot of f44 vs. f43 and a Van Krevelen (V-K) diagram (H:C vs. O:C) were used to explore the degree of oxidation of OA. Ng et al. (2010) used a triangular plot to visualize the relative contributions of CO_2^+ (m/z 44) and $C_2H_3O^+/C_2H_7^+$ (m/z 43). With increasing degree of oxidation of OA, the points in the triangle gather up and move to the top of the triangle. Heald et al. (2010) placed the HR-AMS-derived H:C and O:C ratios in the V-K diagram to infer compositional changes due to different chemical processes. Kroll et al. (2011) utilized the H:C and O:C ratios to estimate the average carbon oxidation state ($OS_c \approx 2\times O:C-H:C$) and used it as a metric to evaluate the degree of oxygenation of organics. The OS_c is also shown in a V-K diagram here. Ng et al. (2011a) showed that ambient OOAs clustered with a slope of about −0.5 in the V-K diagram and OS_c of −1.5 to 1.0 in the carbon oxidation state space. The OS_c field is fitted with points.

Figs. 11 and 12 support the conclusion that the degree of oxidation of OA decreases as RH increases, and this highlights the importance of wet scavenging for OOA. Fig. 11 shows an increase at low RH and a decrease at high RH, which is similar to SV-OOA in Fig. 3, and shares the same explanation. In Fig. 12, the intercept and slope of the regression line are 2.14 and −0.87, respectively. The best-fit line in the work of Heald et al. (2010) has an intercept of 2 (when O:C=0, H:C=2), and it is assumed that SOA precursors are alkenes (only one C=C double bond), cycloalkanes, or arbitrarily long acyclic alkanes. Our intercept is a little higher than 2, which suggests that the SOA precursors in our study comprise the above components mixed with a small amount of alkanes. The slope of the fitted line can be used to infer the composition of OA and the chemical processes in OA formation (Heald et al., 2010; Ng et al., 2011a). The slope is −0.87 here, which is between −0.5 (Ng et al., 2011a) and −1 (Heald et al., 2010), suggesting carboxylic acid formation with and without fragmentation.

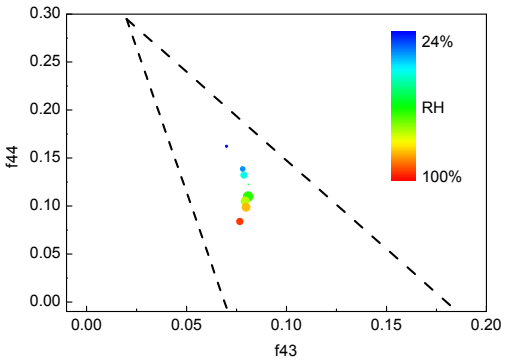

Fig. 11 f44 vs. f43 colored by RH

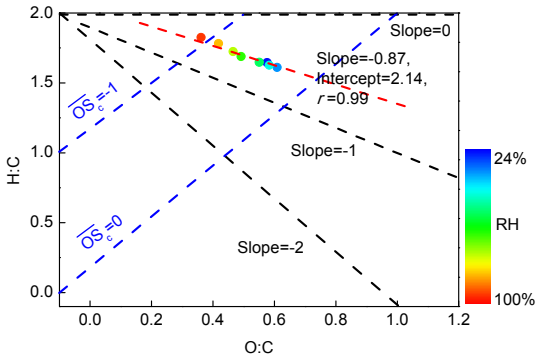

Fig. 12 Van Krevelen diagram (H:C vs. O:C)

4 Conclusions

In this study, the impact of RH on aerosol composition, size distribution, and aging processes were examined in Hangzhou from Aug. 5 to Sept. 23, 2016. Most measurements show a high correlation with RH. Nitrate and chlorine mass concentrations and mass fractions continuously increase with increasing RH. However, many species show differences between low RH and high RH conditions (divided at RH=60%). When RH<60%, organics show a rapid rate of increase when all other factors are increasing. While OOA (LV-OOA and SV-OOA) increase is due to the oxidation of OA, POA increase is due to a slight accumulation in particles. It is notable that SV-OOA shows a significant difference between the day and night means, indicating that the aqueous phase process and a synergistic photochemical effect promote oxygenated SV-OOA formation. When RH>60%, organics show a relatively slow rate of decrease as OOA is predominantly removed by the wet removal effect rather than oxidation, while POA

is still accumulated. The mechanism of POA accumulation requires further study. Sulfate also shows a decreasing tendency, assuming that wet removal overwhelms aqueous phase oxidation.

In NR-PM_1, all species show a peak size growth as RH increases. The organic and sulfate peak size mass concentrations become lower while the mass concentrations of other species, especially nitrate, become higher as a consequence of the wet removal effect on OOA and sulfate and aqueous-phase process enhancing nitrate formation. The pH of the particles seems to be a little alkaline without observed effect of RH. SOR and NOR were at a low level showing little effect of RH, because of the fact that the total emission level is relatively low in this period. NH_4NO_3 replaces $(NH_4)_2SO_4$ as the dominant pattern of ammonium fixation with increasing RH. This study was performed in an ammonium-rich region, which means that nitrate increase via the gas-phase homogeneous reaction between ambient ammonia and nitric acid is significant. Nitrate is the most significant species leading to aerosol growth when RH>60%, and this is therefore a good prospect for controlling emissions of NO_x.

This study was not influenced by emissions from biomass burning. Based on the regression intercept and slope in the V-K diagram, SOA precursors are assumed to be alkenes (only one C=C double bond), cycloalkanes, or arbitrarily long acyclic alkanes mixed with small amounts of alkanes, while the oxidation reaction of OA is carboxylic acid formation with and without fragmentation.

References

Aiken AC, Salcedo D, Cubison MJ, et al., 2009. Mexico City aerosol analysis during MILAGRO using high resolution aerosol mass spectrometry at the urban supersite (T0)—Part 1: fine particle composition and organic source apportionment. *Atmospheric Chemistry & Physics*, 9(17): 6633-6653. https://doi.org/10.5194/acp-9-6633-2009

Aiken AC, Foy BD, Wiedinmyer C, et al., 2010. Mexico City aerosol analysis during MILAGRO using high resolution aerosol mass spectrometry at the urban supersite (T0)—Part 2: analysis of the biomass burning contribution and the modern carbon fraction. *Atmospheric Chemistry & Physics*, 10(12):5315-5341.

Alfarra MR, Prevot AS, Szidat S, et al., 2007. Identification of the mass spectral signature of organic aerosols from wood burning emissions. *Environmental Science & Technology*, 41(16):5770-5777. https://doi.org/10.1021/es062289b

Canagaratna MR, Jayne JT, Jimenez JL, et al., 2007. Chemical and microphysical characterization of ambient aerosols with the aerodyne aerosol mass spectrometer. *Mass Spectrometry Reviews*, 26(2):185-222. https://doi.org/10.1002/mas.20115

Chakraborty A, Gupta T, Tripathi SN, 2016. Combined effects of organic aerosol loading and fog processing on organic aerosols oxidation, composition, and evolution. *Science of the Total Environment*, 573:690-698.

Collett JL, Herckes P, Youngster S, et al., 2008. Processing of atmospheric organic matter by California radiation fogs. *Atmospheric Research*, 87(3-4):232-241. https://doi.org/10.1016/j.atmosres.2007.11.005

Davidson CI, Phalen RF, Solomon PA, 2005. Airborne particulate matter and human health: a review. *Aerosol Science and Technology*, 39(8):737-749. https://doi.org/10.1080/02786820500191348

Day DE, Malm WC, 2001. Aerosol light scattering measurements as a function of relative humidity: a comparison between measurements made at three different sites. *Atmospheric Environment*, 35(30):5169-5176. https://doi.org/10.1016/S1352-2310(01)00320-X

Decarlo PF, 2008. Fast airborne aerosol size and chemistry measurements above Mexico City and Central Mexico during the MILAGRO campaign. *Atmospheric Chemistry and Physics*, 8(14):4027-4048. https://doi.org/10.5194/acp-8-4027-2008

Decarlo PF, Slowik JG, Worsnop DR, et al., 2004. Particle morphology and density characterization by combined mobility and aerodynamic diameter measurements. Part 1: theory. *Aerosol Science & Technology*, 38(12):1185-1205. https://doi.org/10.1080/027868290903907

Decarlo PF, Kimmel JR, Trimborn A, et al., 2006. Field-deployable, high-resolution, time-of-flight aerosol mass spectrometer. *Analytical Chemistry*, 78(24):8281-8289. https://doi.org/10.1021/ac061249n

Ervens B, Turpin BJ, Weber RJ, 2011. Secondary organic aerosol formation in cloud droplets and aqueous particles (aqSOA): a review of laboratory, field and model studies. *Atmospheric Chemistry & Physics*, 11(8): 11(21), 11069-11102. https://doi.org/10.5194/acp-11-11069-2011

Fu Q, Zhuang G, Wang J, et al., 2008. Mechanism of formation of the heaviest pollution episode ever recorded in the Yangtze River Delta, China. *Atmospheric Environment*, 42(9):2023-2036. https://doi.org/10.1016/j.atmosenv.2007.12.002

Gao S, Ng NL, Keywood M, et al., 2004. Particle phase acidity and oligomer formation in secondary organic aerosol. *Environmental Science & Technology*, 38(24):6582-6589. https://doi.org/10.1021/es049125k

Ge X, Zhang Q, Sun Y, et al., 2012. Effect of aqueous-phase processing on aerosol chemistry and size distributions in Fresno, California, during wintertime. *Environmental Chemistry*, 9(3):221-235. https://doi.org/10.1071/EN11168

Gilardoni S, Massoli P, Giulianelli L, et al., 2014. Fog scavenging of organic and inorganic aerosol in the Po Valley. *Atmospheric Chemistry & Physics*, 14(13):6967-6981. https://doi.org/10.5194/acp-14-6967-2014

Hallquist M, Wenger JC, Baltensperger U, et al., 2009. The formation, properties and impact of secondary organic aerosol: current and emerging issues. *Atmospheric Chemistry and Physics*, 9(14):5155-5236. https://doi.org/10.5194/acp-9-5155-2009

He K, Zhao Q, Ma Y, et al., 2012. Spatial and seasonal variability of $PM_{2.5}$ acidity at two Chinese megacities: insights into the formation of secondary inorganic aerosols. *Atmospheric Chemistry & Physics*, 12(3):1377-1395. https://doi.org/10.5194/acp-12-1377-2012

He LY, Lin Y, Huang XF, et al., 2010. Characterization of high-resolution aerosol mass spectra of primary organic aerosol emissions from Chinese cooking and biomass burning. *Atmospheric Chemistry & Physics*, 10(23): 11535-11543. https://doi.org/10.5194/acp-10-11535-2010

Heald CL, Kroll JH, Jimenez JL, et al., 2010. A simplified description of the evolution of organic aerosol composition in the atmosphere. *Geophysical Research Letters*, 37(8):162-169. https://doi.org/10.1029/2010GL042737

Hennigan CJ, Bergin MH, Russell AG, et al., 2009. Gas/Particle partitioning of water-soluble organic aerosol in Atlanta. *Atmospheric Chemistry & Physics Discussions*, 9(11):3613-3628. https://doi.org/10.5194/acp-9-3613-2009

Huang X, Qiu R, Chan CK, et al., 2011. Evidence of high $PM_{2.5}$ strong acidity in ammonia-rich atmosphere of Guangzhou, China: transition in pathways of ambient ammonia to form aerosol ammonium at $[NH_4^+]/[SO_4^{2-}]$ =1.5. *Atmospheric Research*, 99(3-4):488-495. https://doi.org/10.1016/j.atmosres.2010.11.021

Jayne JT, Worsnop DR, Kolb CE, et al., 2000. Development of an aerosol mass spectrometer for size and composition analysis of submicron particles. *Aerosol Science & Technology*, 33(1-2):49-70. https://doi.org/10.1080/027868200410840

Jimenez JL, Canagaratna MR, Donahue NM, et al., 2009. Evolution of organic aerosols in the atmosphere. *Science*, 326(5959):1525-1529. https://doi.org/10.1126/science.1180353

Kanakidou M, Seinfeld JH, Pandis SN, et al., 2005. Organic aerosol and global climate modelling: a review. *Atmospheric Chemistry and Physics*, 5(4):1053-1123. https://doi.org/10.5194/acp-5-1053-2005

Kaul DS, Gupta T, Tripathi SN, et al., 2011. Secondary organic aerosol: a comparison between foggy and nonfoggy days. *Environmental Science & Technology*, 45(17):7307-7313. https://doi.org/10.1021/es201081d

Kroll JH, Donahue NM, Jimenez JL, et al., 2011. Carbon oxidation state as a metric for describing the chemistry of atmospheric organic aerosol. *Nature Chemistry*, 3(2): 133-139. https://doi.org/10.1038/nchem.948

Lanz VA, Alfarra MR, Baltensperger U, et al., 2007. Source apportionment of submicron organic aerosols at an urban site by linear unmixing of aerosol mass spectra. *Atmospheric Chemistry & Physics*, 6(6):11681-11725.

Lim YB, Tan Y, Perri MJ, et al., 2010. Aqueous chemistry and its role in secondary organic aerosol (SOA) formation. *Atmospheric Chemistry & Physics Discussions*, 10(21): 10521-10539. https://doi.org/10.5194/acp-10-10521-2010

Matthew BM, Middlebrook AM, Timothy BO, 2008. Collection efficiencies in an aerodyne aerosol mass spectrometer as a function of particle phase for laboratory generated aerosols. *Aerosol Science & Technology*, 42(11):884-898. https://doi.org/10.1080/02786820802356797

Middlebrook AM, Bahreini R, Jimenez JL, et al., 2012. Evaluation of composition-dependent collection efficiencies for the aerodyne aerosol mass spectrometer using field data. *Aerosol Science & Technology*, 46(3):258-271. https://doi.org/10.1080/02786826.2011.620041

Middleton P, Kiang CS, Mohnen VA, 1980. Theoretical estimates of the relative importance of various urban sulfate aerosol production mechanisms. *Atmospheric Environment*, 14(4):463-472. https://doi.org/10.1016/0004-6981(80)90211-5

Mohr C, Huffman A, Cubison MJ, et al., 2009. Characterization of primary organic aerosol emissions from meat cooking, trash burning, and motor vehicles with high-resolution aerosol mass spectrometry and comparison with ambient and chamber observations. *Environmental Science & Technology*, 43(7):2443-2449. https://doi.org/10.1021/es8011518

Ng NL, Canagaratna MR, Zhang Q, et al., 2010. Organic aerosol components observed in Northern Hemispheric datasets from Aerosol Mass Spectrometry. *Atmospheric Chemistry and Physics*, 10(10):4625-4641. https://doi.org/10.5194/acp-10-4625-2010

Ng NL, Canagaratna MR, Jimenez JL, et al., 2011a. Changes in organic aerosol composition with aging inferred from aerosol mass spectra. *Atmospheric Chemistry & Physics*, 11(13):6465-6474. https://doi.org/10.5194/acp-11-6465-2011

Ng NL, Canagaratna MR, Jimenez JL, et al., 2011b. Real-time methods for estimating organic component mass concentrations from aerosol mass spectrometer data. *Environmental Science & Technology*, 45(3):910-916. https://doi.org/10.1021/es102951k

Ortega AM, Hayes PL, Peng Z, et al., 2016. Real-time measurements of secondary organic aerosol formation and aging from ambient air in an oxidation flow reactor in the Los Angeles area. *Atmospheric Chemistry & Physics*, 16(11):7411-7433. https://doi.org/10.5194/acp-16-7411-2016

Paatero P, Tapper U, 1994. Positive matrix factorization: a non-negative factor model with optimal utilization of error estimates of data values. *Environmetrics*, 5(2): 111-126. https://doi.org/10.1002/env.3170050203

Pathak RK, Louie PKK, Chan CK, 2004. Characteristics of aerosol acidity in Hong Kong. *Atmospheric Environment*, 38(19):2965-2974. https://doi.org/10.1016/j.atmosenv.2004.02.044

Pathak RK, Wu WS, Wang T, 2009. Summertime PM2.5 ionic species in four major cities of China: nitrate formation in an ammonia-deficient atmosphere. *Atmospheric Chemistry and Physics*, 9(5):1711-1722. https://doi.org/10.5194/acp-9-1711-2009

Saxena P, Seigneur C, 1987. On the oxidation of SO_2 to sulfate in atmospheric aerosols. *Atmospheric Environment*, 21(4):807-812. https://doi.org/10.1016/0004-6981(87)90077-1

Schneider J, Weimer S, Drewnick F, et al., 2006. Mass spectrometric analysis and aerodynamic properties of various types of combustion-related aerosol particles. *International Journal of Mass Spectrometry*, 258(1-3):37-49. https://doi.org/10.1016/j.ijms.2006.07.008

Seigneur C, Saxena P, 1988. A theoretical investigation of sulfate formation in clouds. *Atmospheric Environment*, 22(1):101-115. https://doi.org/10.1016/0004-6981(88)90303-4

Seinfeld JH, Pandis SN, 2012. Atmospheric Chemistry and Physics: from Air Pollution to Climate Change, 2nd Edition. John Wiley & Sons, USA.

Seinfeld JH, Erdakos GB, Asher WE, et al., 2001. Modeling the formation of secondary organic aerosol (SOA). 2. The predicted effects of relative humidity on aerosol formation in the alpha-pinene-, beta-pinene-, sabinene-, delta 3-carene-, and cyclohexene-ozone systems. *Environmental Science & Technology*, 35(9):1806-1817. https://doi.org/10.1021/es001765+

Shen X, Lee T, Guo J, et al., 2012. Aqueous phase sulfate production in clouds in eastern China. *Atmospheric Environment*, 62(15):502-511. https://doi.org/10.1016/j.atmosenv.2012.07.079

Solomon S, 2007. Climate Change 2007-the Physical Science Basis: Working Group I Contribution to the Fourth Assessment Report of the IPCC (Vol. 4). Cambridge University Press, UK.

Squizzato S, Masiol M, Brunelli A, et al., 2013. Factors determining the formation of secondary inorganic aerosol: a case study in the Po Valley (Italy). *Atmospheric Chemistry and Physics*, 13(4):1927-1939. https://doi.org/10.5194/acp-13-1927-2013

Sun Y, Zhuang G, Tang AA, et al., 2006. Chemical characteristics of $PM_{2.5}$ and PM_{10} in haze-fog episodes in Beijing. *Environmental Science & Technology*, 40(10): 3148-3155. https://doi.org/10.1021/es051533g

Sun Y, Wang Z, Fu P, et al., 2013. The impact of relative humidity on aerosol composition and evolution processes during wintertime in Beijing, China. *Atmospheric Environment*, 77(3):927-934. https://doi.org/10.1016/j.atmosenv.2013.06.019

Tkacik DS, Lambe AT, Jathar S, et al., 2014. Secondary organic aerosol formation from in-use motor vehicle emissions using a potential aerosol mass reactor. *Environmental Science & Technology*, 48(19):11235-11242. https://doi.org/10.1021/es502239v

Tong Z, Whitlow TH, Landers A, et al., 2015. A case study of air quality above an urban roof top vegetable farm. *Environmental Pollution*, 208(Part A):256-260.

Tong Z, Chen Y, Malkawi A, et al., 2016a. Energy saving potential of natural ventilation in China: the impact of ambient air pollution. *Applied Energy*, 179(1):660-668.

Tong Z, Chen Y, Malkawi A, 2016b. Defining the Influence Region in neighborhood-scale CFD simulations for natural ventilation design. *Applied Energy*, 182:625-633.

Tong Z, Yang B, Hopke PK, et al., 2017. Microenvironmental air quality impact of a commercial-scale biomass heating system. *Environmental Pollution*, 220(Part B):1112-1120. https://doi.org/10.1016/j.envpol.2016.11.025

Ulbrich IM, Canagaratna MR, Zhang Q, et al., 2008. Interpretation of organic components from positive matrix factorization of aerosol mass spectrometric data. *Atmospheric Chemistry & Physics*, 8(2):2891-2918. https://doi.org/10.5194/acpd-8-6729-2008

Wong JPS, Lee AKY, Slowik JG, et al., 2011. Oxidation of ambient biogenic secondary organic aerosol by hydroxyl radicals: effects on cloud condensation nuclei activity. *Geophysical Research Letters*, 38(22):178-181. https://doi.org/10.1029/2011GL049351

Zhang Q, Jimenez JL, Worsnop DR, et al., 2007a. A case study of urban particle acidity and its influence on secondary organic aerosol. *Environmental Science & Technology*, 41(9):3213-3219. https://doi.org/10.1021/es061812j

Zhang Q, Jimenez JL, Canagaratna MR, et al., 2007b. Ubiquity and dominance of oxygenated species in organic aerosols in anthropogenically-influenced Northern Hemisphere midlatitudes. *Geophysical Research Letters*, 34(13): L13801. https://doi.org/10.1029/2007GL029979

Zhang Q, Jimenez JL, Canagaratna MR, et al., 2011. Understanding atmospheric organic aerosols via factor analysis of aerosol mass spectrometry: a review. *Analytical & Bioanalytical Chemistry*, 401(10):3045-3067. https://doi.org/10.1007/s00216-011-5355-y

List of electronic supplementary materials

Fig. S1 Variations as a function of RH. Data are binned based on RH, and the median (horizontal line), mean (little square box), 75th and 25th (box upper and lower range), outlier with coefficient 1.5 (lower and upper whiskers), and 99th and 1st (upper and lower crosses), maximum, and minimum are shown

Fig. S2 PMF results for four factors' mass concentrations vs. time series and four factors' mass spectra

Fig. S3 Relationships of different species size distributions with RH. Color bar means the mass concentration

中文概要

题　目： 中国杭州夏季相对湿度对难溶性的亚微米级气溶胶演化的影响

目　的： 研究湿度对气溶胶的影响。

创新点： 首次研究气溶胶中铵盐的存在形式，为研究相对湿度对大气中气溶胶的影响做了补充。

方　法： 1. 利用高分辨飞行时间气溶胶质谱仪采集的外场数据分析各组分时序浓度和粒径分布，并通过正矩阵因数分解模型进行来源解析。2. 通过研究各种物质和解析的因子随湿度的变化，探讨湿度对气溶胶演化的影响。3. 通过相关性处理探究铵在气溶胶中的存在形式。

结　论： 在相对湿度大于 60%时，湿祛除效应对有机物中的二次有机气溶胶及硫酸盐的影响较大，而硝酸盐受液相反应生成作用影响更大。湿度从低到高时，气溶胶中铵的存在形式由硫酸铵向硝酸铵过渡。

关键词： 相对湿度；气溶胶组成；粒径分布；湿法去除；液相反应